

A new tool for evaluating the physics of coupled atmosphere–ocean variability in nature and in general circulation models

William H. G. Roberts · David S. Battisti

Received: 8 July 2009 / Accepted: 3 February 2010 / Published online: 13 March 2010
© Springer-Verlag 2010

Abstract Intermediate models of the coupled tropical atmosphere–ocean system have been used to illuminate the physics of interannual climate phenomenon such as El Niño Southern Oscillation (ENSO) in the tropical Pacific and to explore how the tropics might respond to a forcing such as changing insolation (Milankovitch) or atmospheric carbon dioxide. Importantly, most of the intermediate models are constructed as anomaly models: models that evolve on a prescribed climatological mean state, which is typically prescribed and done so on a rather ad hoc basis. Here we show how the observed climatological mean state fields [ocean currents and upwelling, sea surface temperature (SST) and atmospheric surface winds] can be incorporated into a linearized intermediate model of the tropical coupled atmosphere–ocean system: called Linear Ocean–Atmosphere Model (LOAM), it is a linearized version of the Zebiak and Cane model. With realistic, seasonally varying mean state fields, we find that the essential physics of the ENSO mode is very similar to that in the original model and to that in the observations and that the observed mean fields support an ENSO mode that is stable to perturbations. Thus, our results provide further evidence that ENSO is generated and maintained by stochastic (uncoupled) perturbations. The method that we have outlined can be used to assimilate any set of ocean and atmosphere

climatological data into the linearized atmosphere–ocean model. In a companion paper, we apply this same method to incorporate mean field output from two global climate models into the linearised model. We use the latter to diagnose the physics of the leading coupled mode (ENSO) that is supported by the climate models, and to illuminate why the structure and variance in the ENSO mode changes in the models when they are forced by early Holocene and Last Glacial Maximum boundary conditions.

Keywords El Niño Southern Oscillation (ENSO) · Tropical climate · Climate models

1 Introduction

Scientists realized in the early 1980s that El Niño, an unusually warm water off the coast of Peru around Christmas time, was often associated with a larger scale ocean phenomenon—a warming of the whole eastern equatorial Pacific—that was concomitant with a perturbation in the nearly global atmospheric phenomenon known as the Southern Oscillation. Today the science community refers to the larger scale coupled phenomenon as ENSO and recognizes it as the leading pattern of natural climate variability on interannual time scales. The early phase of research (the 1980s) on the ENSO phenomenon was carried out at a time when coupled atmosphere–ocean general circulation models barely existed and were prohibitively expensive to run.¹

¹ The first integration using an atmosphere–ocean general circulation model that showed a ENSO event similar to those observed was performed in 1990 by Philander et al. (1992). This was a single 28 year simulation (albeit with a crude resolution in the atmosphere by today's standards) performed on one of the fastest machines available at the time.

W. H. G. Roberts · D. S. Battisti (✉)
Department of Atmospheric Sciences, University of Washington,
Seattle, WA, USA
e-mail: battisti@u.washington.edu

Present Address:
W. H. G. Roberts
School of Geographical Sciences, University of Bristol,
Bristol BS8 1SS, UK
e-mail: wroberts@atmos.washington.edu

Thus, much of the early research on ENSO utilized “intermediate” coupled atmosphere–ocean models that, for reasons of efficiency, were designed to exclude physics that were thought to be irrelevant for ENSO and to resolve physics that were thought (and later confirmed) to be important for ENSO, including finer meridional resolution in the equatorial Pacific ocean than was used at the time.

Much was learned from the experiments using intermediate models of the coupled tropical atmosphere–ocean system. For example, as suggested by the tight coordination between the large scale sea surface temperature (SST) and atmospheric circulation anomalies in the observations, ENSO was shown to be due to coupling between the atmosphere and the ocean within the tropical Pacific, and is best described as a true mode of the (linearized) coupled atmosphere–ocean system. Intermediate models also showed that the temporal and spatial structure of the ENSO mode was extremely sensitive to the structure of the climatological mean state in the tropical Pacific atmosphere and ocean, as was the stability of the ENSO mode.

A dozen or so studies in the 1990s reported results from coupled atmosphere–ocean general circulation models that featured realistic ENSO-like behavior; the essential physics in the general circulation models was similar to that found in the intermediate coupled atmosphere–ocean models. In general, these studies featured models that had a better representation of the ocean physics (in particular, enhanced resolution in the ocean near the equator) and applied flux corrections to maintain realistic climatological mean states—shown to be important in studies using intermediate coupled models and in studies of the linear coupled modes. Neelin et al. (1998) present a synthesis review of ENSO theory.

Since the mid-1990s these climate models have continued to evolve and many new coupled atmosphere–ocean general circulation models have been built. A primary reason for the development of these models is to study the response of the climate system to anthropogenic forcing. Hence, most of these models are void of flux corrections which in the past were employed to ensure that the simulated modern day climate state is very similar to that observed. For most applications, this is not a problem. Theory and experience with the intermediate models and general circulation models suggests, however, that whether a climate model will support ENSO variability is dependent on having a highly realistic climatological mean state. Thus, it is not surprising that only two to four of the 23 models used in the most recent Intergovernmental Panel on Climate Change (IPCC) 2007 scientific Assessment Report (AR4) support realistic ENSO variability (e.g., van Oldenborgh et al. 2005; Guilyardi et al. 2009).

A major advantage that the intermediate models have for capturing ENSO is that they are usually cast as anomaly

models about a prescribed climatological mean state. While there were arguably sufficient data to determine the climatology in wind and SST in the tropical Pacific by 1980, there were insufficient data to define even qualitatively the climatological mean state in ocean currents and upwelling—which the intermediate models featured as essential to the ENSO mode. Thus, a major advantage of the intermediate models is also their Achilles heel: these models showed that the nature of the coupled variability is extremely sensitive to the mean state and for some fields the mean states prescribed in these models are poor approximations of reality. As an example, consider the Zebiak and Cane model (Zebiak and Cane 1987, hereafter ZCM)—an early intermediate model that is still in widespread use. During the late 1980s, when the ZCM was first written, the climatological SST and wind stress were reasonably well known, but the temperature beneath the surface was not well observed. Furthermore, ocean current measurements in the Pacific ocean basin were virtually non-existent. This lack of observations meant that in order to have a full set of background states to prescribe in the model, Zebiak and Cane (1987) needed to make some approximations. The mean ocean currents and upwelling were estimated by forcing the 1.5 layer ocean model in the ZCM with the RC climatological wind stress from (Rasmusson and Carpenter 1982, hereafter referred to as RC); the necessary subsurface temperature parameterisations were devised on an ad hoc basis.

Now, twenty-some years after the model was written, the tropical Pacific Ocean is much better observed. The TAO array, McPhaden et al. (1998) makes real-time measurements of the ocean temperature within 10° of the equator, from the western to eastern Pacific, to depths of hundreds of metres. Satellite measurements provide observations of the wind stress and SST, and a number of model-data assimilation products also provide ocean current data. With all these new data we can now prescribe background states and subsurface parameterisations that far more accurately represent the mean state of the tropical Pacific than those that were originally used in the ZCM or other intermediate models for studying ENSO. To our knowledge, none of the intermediate models that have been published make use of the (more recent) data that better constrain the climatological mean states that are important for ENSO.

In this paper we describe how these new observational data may be used to make new sets of background states that can be inserted into a linearised version of the ZCM.

The necessary parameterizations are adjusted in stand-alone, uncoupled simulations of ocean and atmosphere components to optimally fit observations. *Hence there are no underlying assumptions about the stability of the coupled system and ENSO in the new linear model.* For that

matter, there is no guarantee that the temporal or spatial structure of the leading mode in coupled system will even be ENSO-like.

The paper is laid out as follows: first we briefly describe the linear coupled model in Sect. 2. We summarize the horizontal data sets that are available for use as horizontal background states in Sect. 3.1 and how these new data differ from the horizontal mean states originally used in the ZCM. In Sect. 3.2 we describe how observational data may be used to derive subsurface parameterisations that determine how the SST is affected by vertical processes. Finally we describe the results of using the aforementioned observed background states in a linearised version of the ZCM in Sect. 4. In a companion paper, we apply this same method to incorporate mean field output from two of the global climate models used in the most recent IPCC Assessment Report into the linearised model and evaluate the physics of the ENSO mode simulated in those models (and the coupled atmosphere–ocean variability in general).

2 Model description

The intermediate model we shall use is the so-called Linear Ocean–Atmosphere Model (LOAM) of Thompson and Battisti (2000). LOAM is the linearized version of the ZCM model used by Battisti (1988) (hereafter, B88M), recast in matrix form by Thompson and Battisti (2000).² The coupled modes supported by the prescribed mean states are found by decomposing the annual propagator matrix into its Floquet modes. [The Floquet modes of this system are the eigenmodes of the (cyclo-stationary) annual propagator matrix, and each mode has an associated period and decay rate that are derived from the eigenvalues of each mode.] As is shown in Thompson and Battisti (2000), the least damped Floquet mode that stems from using the mean states prescribed in the B88M (and the ZCM) features temporal and spatial characteristics that are very similar to those associated with the observed canonical ENSO; thus this mode is termed the ENSO mode.

Thompson and Battisti (2000) showed that the ENSO mode in LOAM using the same background states and parameterisations as in B88M is unstable. However, they noted that a number of the parameters used in B88M were not realistic. Specifically, the western boundary reflection and ocean mechanical damping used in B88M were both larger than those observed. When LOAM was rerun with more realistic values of the western boundary reflection and ocean damping, in a version of LOAM called T80, the leading mode was still very similar to the observed ENSO,

in both spatial and temporal structure, but it was now stable.

3 New mean state and parameterisation calculation

Linear Ocean–Atmosphere Model is linearized about a prescribed climatological mean state, including the annual cycle. Mean state variables that are required include SST, surface winds, upper ocean currents and upwelling. In the subsections that follow, we describe how the observed mean state fields are incorporated into LOAM. For these sections to be meaningful, however, we first must introduce and discuss the equation that governs SST in the ZCM. The ZCM includes an ocean thermodynamic equation for the surface layer of the ocean, taken to be the top 50 m. In LOAM the linearisation of the SST tendency equation for this layer is written (see Thompson 1998, for more details):

$$\frac{\partial T}{\partial t} = -u_1 \frac{\partial \bar{T}}{\partial x} - v_1 \frac{\partial \bar{T}}{\partial y} - \left[\bar{u}_1 \frac{\partial}{\partial x} + \bar{v}_1 \frac{\partial}{\partial y} \right] T - K_w(x, y)w_1 - K_T(x, y)h - d(x, y)T, \quad (1)$$

where

$$K_w(x, y) \equiv \delta_w H_m \bar{T}_z H(\bar{w}_1), \quad (2)$$

with $H(x)$ the Heaviside function:

$$H(x) \equiv \begin{cases} 0, & \text{when } x < 0 \\ 1, & \text{when } x \geq 0. \end{cases} \quad (3)$$

The coefficient K_T is given by

$$K_T(x, y) \equiv -\delta_T \frac{\Delta(\bar{w}_1)}{H_m} \Gamma(x), \quad (4)$$

where

$$\Gamma(x) = \frac{\partial T_s}{\partial h} \Big|_{h=0} \quad (5)$$

and

$$d(x, y) = \alpha_s + \delta_T \frac{\Delta(\bar{w}_1)}{H_m}, \quad (6)$$

where

$$\Delta(x) \equiv \begin{cases} 0, & \text{when } x < 0 \\ x, & \text{when } x \geq 0. \end{cases} \quad (7)$$

Variables with an overbar represent time averaged background state quantities (which includes the annual cycle), and unadorned variables represent deviations from the climatological annual cycle calculated by the model. u_1 , v_1 and w_1 are the surface layer currents: zonal, meridional and vertical, respectively. T is the SST and h is the upper layer depth anomaly. \bar{T}_z is the mean vertical temperature gradient at the base of the surface layer and $T_s(h)$ the

² There are minor differences between the B88M version of the ZCM and the original ZCM; see Mantua and Battisti (1995) for details.

anomalous temperature there: this is a function of the thermocline depth h , expressed in terms of the depth of the upper layer of the 1.5 layer model. We will discuss $T_s(h)$ and \overline{T}_z in more detail below. δ_w and δ_T are so called efficiency factors that represent a raft of processes absent the 1.5 layer model: there is more discussion of these two terms in Sect. 3.2.3. α_s^{-1} is the parameterization of the thermal damping by the surface fluxes, set to a value of 125 days. Finally $H_m = 50\text{m}$ is the surface layer depth. See Seager et al. (1988) for more discussion of the SST equation in the ZCM, and Thompson (1998) for more discussion on the linearisation of the SST equation.

The first four terms on the right hand side of Eq. 3 represent horizontal advection. The next term, involving $K_w(x, y)$, represents the effect of the anomalous upwelling w_1 of the mean temperature gradient. The penultimate term in Eq. 3, which involves $K_T(x, y)$, represents the effect of the mean upwelling of the anomalous temperature gradient. Finally, $d(x, y)$ is a damping term.

The climatological mean state quantities \overline{u}_1 , \overline{v}_1 , \overline{w} , and \overline{T} are specified from data, as discussed in the next section. The climatological mean states of $T_s(h)$ and \overline{T}_z are presented in Sect. 3.2.

3.1 The climatological ocean currents and surface temperature

The horizontal background states required by LOAM are derived by calculating monthly averages from the observed data and interpolating them onto the LOAM atmosphere and ocean grids. The background states required are: surface winds, the vertical structure of the ocean temperature along the equator, SST and surface ocean currents. In this study we shall use a number of different observational datasets to determine these background states. We shall begin by outlining the differences between RC background states originally used in the ZCM and background states from the most up-to-date observations. In general we shall only graphically depict the differences between one of the new mean state products and the original mean state products because the differences between the climatologies in new and old data sets are greater than the differences between the various new data sets.

Available surface wind products are from Florida State University (Bourassa et al. 2001, hereafter referred to as FSU) and the NCEP reanalysis³ (Kalnay et al. 1996); the latter are shown in Fig. 1b, e. There are significant differences between these two datasets and the RC climatology that was originally used in ZCM. For example, we see

that the easterly Trade winds from NCEP are stronger than the RC Trades (c.f., Fig. 1a–c; similarly, the FSU Trade winds are also stronger than the RC Trade winds (not shown). In Fig. 1d–f we see that the NCEP meridional winds are also stronger than their RC counterparts. As has been commented upon elsewhere (Wittenberg 2004) there are also differences between the FSU and NCEP wind products themselves, although the differences between the modern wind products are small compared to the difference between the RC product and either of the modern products.

Sea surface temperature is available from the Simple Ocean Data Assimilation (Carton et al. 2000a, b, hereafter referred to as SODA) shown in Fig. 1h and the NCEP/OI data⁴ (Reynolds et al. 2002, not shown). We see that the SODA product features a much stronger cold tongue than the original SST product used in ZCM (Fig. 1g): this gives a stronger zonal temperature gradient (Fig. 1i). The SST from the NCEP/OI data set is very similar to that from SODA, with any differences between NCEP/OI and SODA being much smaller than the difference between either reanalysis product and the RC product.

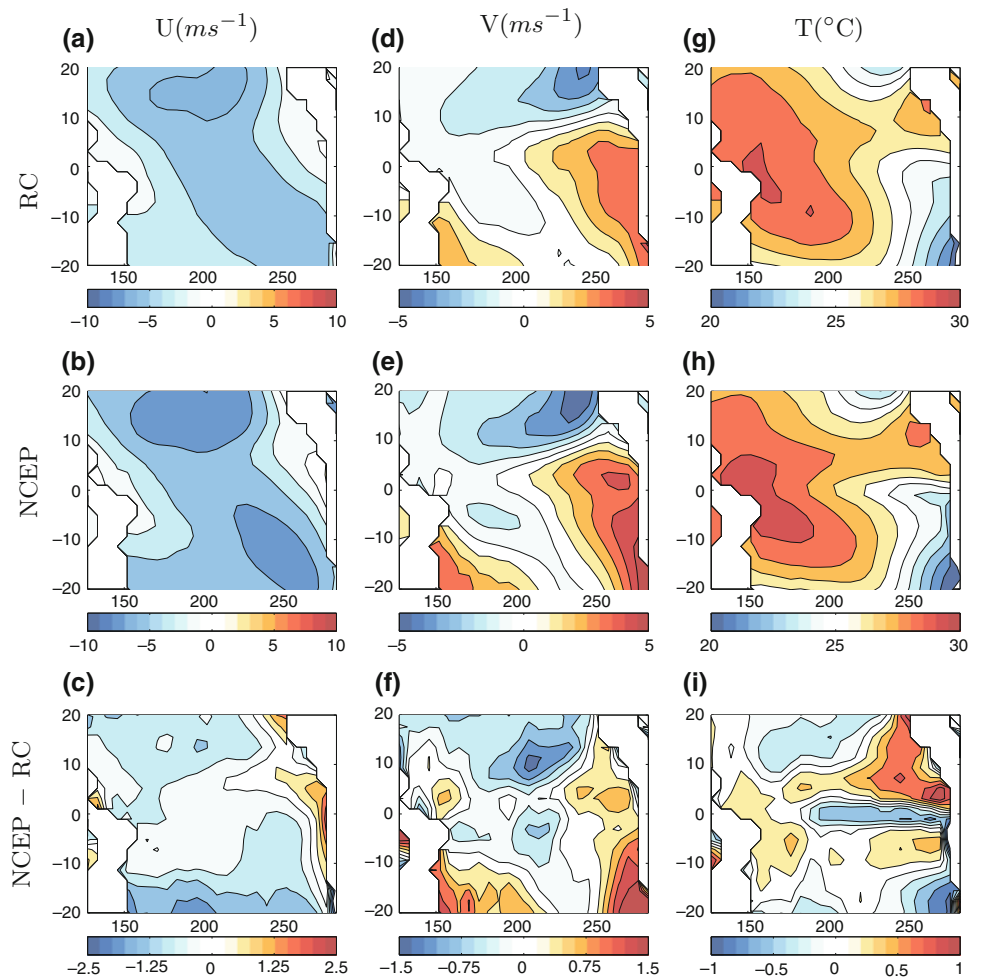
The background state currents that are needed are averages over the top 50 m of the ocean—the depth of the surface layer that is embedded in the 1.5 layer ocean in ZCM. Surface currents are more difficult to measure than either wind stress or SST, consequently background states for these are from data assimilation products. The two assimilation products that we shall use are SODA (Carton et al. 2000a, b) and the Global Ocean Data Assimilation System (Behringer and Xue 2004, hereafter referred to as GODAS). Both assimilation products incorporate available observations of temperature, the climatological salinity, the observed winds and various surface fluxes to produce full three dimensional current and temperature fields. Although surface current measurements are available from drifters and buoys, we chose to use the currents from the data assimilation products because the current data are available throughout the equatorial domain and are available throughout the upper 50 m. Two independent assimilation products will be used in order to obtain a sense of the sensitivity of the leading mode in the coupled system to differences in the currents. Recall that the background ocean currents in the original in ZCM were computed using the 1.5 layer ocean model forced by the RC winds. Hence the original ZCM currents present a much cruder representation of the currents than the data assimilation products.

The zonal currents from SODA, in Fig. 2b, show that there is westward flow flanking the equator and eastward flow along the equator. This is very different to the currents

³ NCEP Reanalysis Derived data provided by the NOAA/OAR/ESRL PSD, Boulder, CO, USA, from their Web site at “<http://www.cdc.noaa.gov>”.

⁴ NOAA_OI_SST_V2 data provided by the NOAA/OAR/ESRL PSD, Boulder, CO, USA, from their Web site at “<http://www.cdc.noaa.gov/>”.

Fig. 1 Annual mean winds and SST. Annual zonal winds from **a** RC, **b** NCEP, and **c** the difference. Annual meridional winds from **d** RC, **e** NCEP and **f** the difference. Annual SST from **g** RC, **h** SODA and **i** the difference SODA-RC

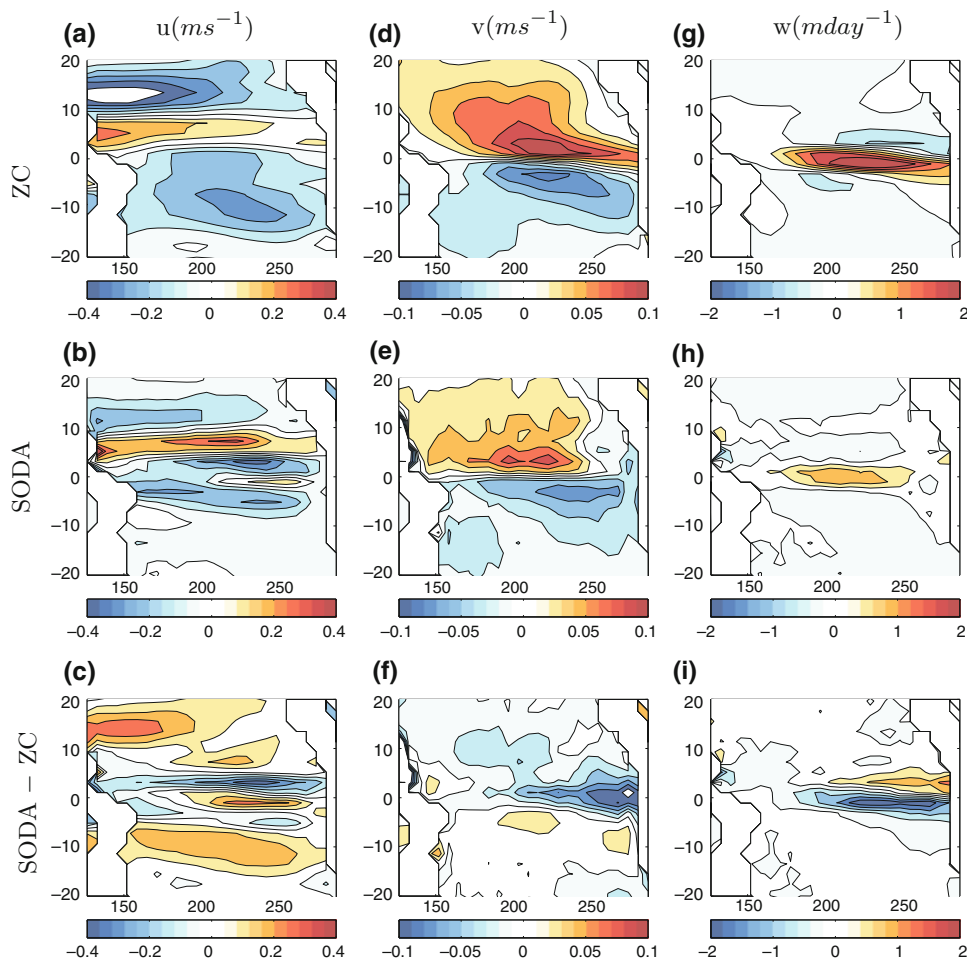


derived from the 1.5 layer ocean model in ZCM, see Fig. 2a. Absent in the ZCM background zonal current is the reversal of the current on the equator at around 250°E; this is the equatorial undercurrent coming to the surface. In the ZCM background state the maximum in the north equatorial counter current is located farther to the west than in either of the assimilation products. Meridional currents in SODA, as shown in Fig. 2e, also differ from the ZCM currents, Fig. 2d, which are too strong in the far eastern Pacific. The strong currents in the ZCM result in large divergence away from the equator and, hence, strong upwelling compared to either of the assimilation products (c.f., Fig. 2g–i). The maximum upwelling in the ZCM is also displaced far to the east compared to the assimilation products. Hence, the differences between the currents and upwelling found in the original ZCM product and those from either the GODAS or SODA products are much greater than those between the two assimilation products. We note also that the amplitude of the upwelling in both assimilation products agrees with that estimated from the moored buoys (Johnson et al. 2001) and from the drifter data (Poullain 1993).

The differences between the currents estimated using the data assimilation products and that produced using the 1.5 layer ocean model (forced by observed winds) are due to differences in the ocean model physics formulations as well as the assimilation of observations in the former cases but not in the latter case. When we take the same wind stress product that is used to create the GODAS assimilation product and use it to force the ocean model used in the ZCM, we obtain climatological currents that are very similar to those used in Zebiak and Cane (1987) (obtained by forcing the ZCM ocean model with the RC winds). Hence we may conclude that the differences in the RC and NCEP wind stress products—although considerable—are not the responsible for the large differences in the original currents and those in either analysis product; rather the differences are due to differences in the ocean models used, and in the data that are assimilated.

We have shown in this section that there are significant differences between the best estimates of the climatological background states and those originally used in B88M. These background states are not the only fields that need to be specified in order to run LOAM, however. There

Fig. 2 Annual mean surface currents from SODA and ZC. Zonal currents from **a** ZC, **b** SODA, and **c** the difference SODA-ZC. Meridional currents from **d** ZC, **e** SODA, and **f** the difference SODA-ZC. Upwelling from **g** ZC, **h** SODA, and **i** the difference SODA-ZC



remains to be specified the two subsurface parameterisations, which were originally derived on a somewhat ad hoc basis; these are discussed next.

3.2 Subsurface mean fields and the parameterisation of ocean entrainment and mixing

We present in this section the climatological mean states of $T_s(h)$ and \overline{T}_z . We use subsurface temperature data from three available data sets: the two previously discussed model-data assimilation products, SODA and GODAS, and the Bureau of Meteorology Research Centre analysis product (Smith 1995a, b, hereinafter referred to as BOM). The BOM product uses direct observations of temperature, including all the available temperature data, such as XBT, CBT and TAO data and interpolates it onto a three dimensional grid.

3.2.1 The mean temperature gradient at the base of the surface layer, \overline{T}_z

Figure 3 shows estimates of \overline{T}_z along the equator from the various ocean temperature data sets. \overline{T}_z is the annual mean

vertical temperature gradient at a depth of 50 m, calculated at all points on the LOAM grid between 127°E–271°E and averaged over 4.5°N–4.5°S. Although \overline{T}_z is really a function of latitude and longitude, Zebiak and Cane (1987) ignored meridional variations in \overline{T}_z for both the sake of simplicity and because of the lack of data. In the present study we retain this simplification and use an average over 4.5°N–4.5°S which represents well the mean equatorial value.

There is broad agreement amongst the various observation-based data sets on the amplitude of \overline{T}_z as we traverse the equator from west to east until around 220°E, where the new values greatly exceed those originally used in B88M.

3.2.2 The temperature anomaly at the base of the surface mixed layer, $T_s(h)$

The term $K_T \cdot h$ in Eq. 1 represents the surface temperature tendency due to mean upwelling of an anomalous temperature gradient. This anomalous temperature gradient arises from anomalies in thermocline depth that create

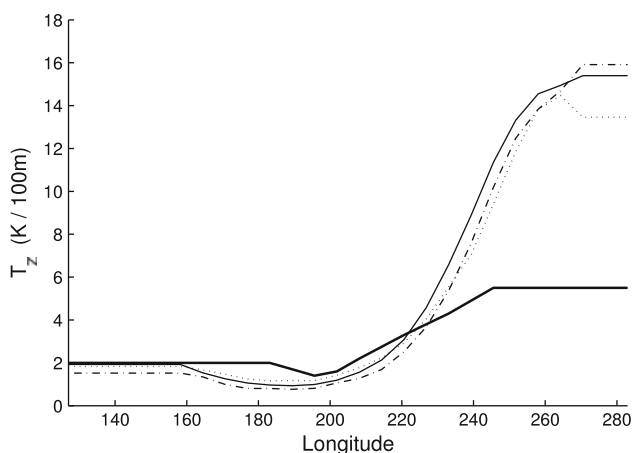


Fig. 3 \bar{T}_z . Bold solid line the ZC original, solid from BOM data, dotted from SODA, dash-dotted from GODAS

anomalies in temperature at the base of the surface layer, T_s , which is taken to be at 50 m.

In the original ZCM and B88M, $T_s(h)$ was approximated by a *tanh* function with two pairs of parameters that were chosen on an ad hoc basis (see Mantua and Battisti 1995, for more discussion). In order to constrain $T_s(h)$ by data, Seager et al. (1988) devised an empirical scheme that fit the depth of the model interface, \tilde{h} , to the observed thermocline depth; the latter was defined as the depth of the 20°C isotherm, h_{20}^* . They then fit h_{20}^* to observed 50 m temperature, T_{50}^* : $T_{50}^* \equiv cs(h_{20}^*)$. Combining these two fits gives a fit of the model interface depth \tilde{h} to the observed 50 m temperature T_{50}^* . Since the base of the surface layer is at a depth of 50 m, this fit is analogous to $T_s(\tilde{h})$. We shall follow this procedure to calculate $T_s(\tilde{h})$ from observations and then use a linearisation of the result in LOAM.

The 1.5 layer ocean model approximates the real ocean thermocline as the interface between the upper and lower model layers. The density change over the real thermocline is a continuous function, whereas in the 1.5 layer model it is a step change. Thus, we would not expect that, for the same wind stress forcing, the interface height in the 1.5 layer model to be at the same as the depth of the thermocline in the real ocean. For this reason a mapping of thermocline depth h_{20}^* to upper layer interface depth \tilde{h} is required. We shall call this mapping $f(\tilde{h})$:

$$h_{20}^* = f(\tilde{h}), \tag{8}$$

where $(\tilde{\quad})$ denotes the total displacement, which is the sum of the climatological annual cycle $(\bar{\quad})$ and the anomaly h about the climatological annual cycle (e.g., $\tilde{h} = \bar{h} + h$). Seager et al. (1988) derive f by fitting the observed annual cycle of thermocline depth, taken as the 20°C isotherm depth, to \bar{h} from the 1.5 layer model forced by the annual cycle of wind stress. For reasons stated in Seager et al. (1988), a quadratic fit is used. Note that the annual cycle in

both h_{20}^* and wind stress is used here to estimate $f(\tilde{h})$: anomalies in \tilde{h} are not included in this calculation (see comment later in this section).

In order to obtain $f(\tilde{h})$ from the new data, we force the 1.5 layer ocean with the wind stress climatologies (both FSU and NCEP) to get the annual cycle of \tilde{h} ($=\bar{h}$). We then calculate the annual cycle of h_{20}^* from each of the ocean temperature datasets (BOM, SODA and GODAS) and fit this to \bar{h} . Thus, 12 pairs of numbers $(\bar{h}, \bar{h}_{20}^*)$ are obtained for each location. This is done for each of 76 (2° latitude by 10° longitude) grid boxes between 4.5°N and 4.5°S from 170°E to 270°E, yielding $12 \times 76 = 912$ pairs of values that define $f(\tilde{h})$.

Figure 4 shows the scatter of points when this is done using \bar{h}_{20}^* calculated from SODA, and \bar{h} computed by forcing the linearised 1.5 layer ocean with the climatology of NCEP wind stress. Other combinations of wind and temperature datasets yield very similar results. Also shown in Fig. 4 is the quadratic fit of the data, which we define as $f(\tilde{h})$.

Next, we define cs to be the function that relates the observed 50 m temperature, T_{50}^* , to the observed thermocline depth, h_{20}^* :

$$T_s \equiv T_{50}^* = cs(h_{20}^*). \tag{9}$$

We estimate cs by plotting T_{50}^* against h_{20}^* for grid boxes along the equator (again, note that the annual cycle of T_{50}^* and h_{20}^* are used; see comment below); this scatter plot is shown in Fig. 5 for the SODA product. A cubic spline with six tie points is then applied to the data to obtain the parameterization for cs ; all three temperature data sets yield very similar curves for cs .

With $cs(h_{20}^*)$ and $f(\tilde{h})$ empirically derived, we now have a function that relates the subsurface temperature to the

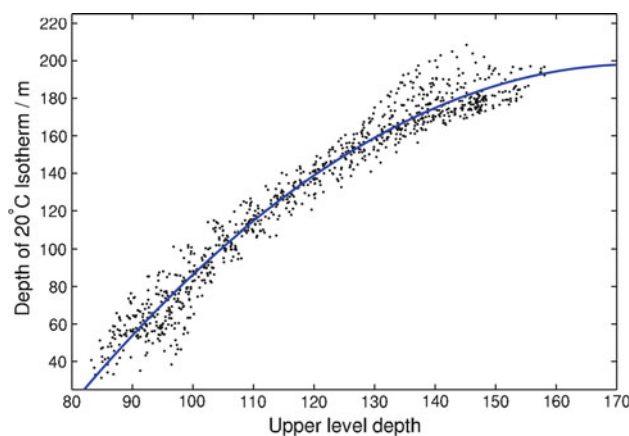


Fig. 4 Scatter plot of upper level depth, \bar{h} , against the observed 20°C isotherm depth, \bar{h}_{20}^* from SODA. Data are plotted for each of 72 (2° latitude by 10° longitude) grid boxes between 4.5°N and 4.5°S from 170°E to 270°E, yielding $12 \times 76 = 912$ pairs of values that define $f(\tilde{h})$. The quadratic fit $f(\tilde{h})$ is also plotted

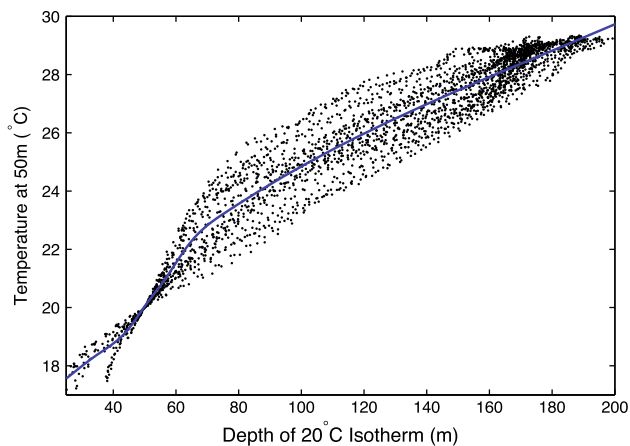


Fig. 5 Scatter plot of observed 50 m temperature, T_{50}^* , against the 20°C isotherm depth, h_{20}^* , for the SODA. The cubic-spline curve fit, $cs(h_{20}^*)$ is also shown

interface height in 1.5 layer ocean model that is constrained by data:

$$T_s(\tilde{h}) = cs(f(\tilde{h})). \tag{10}$$

Linearizing about the climatological mean state $(\bar{h}, \bar{h}_{20}^*)$, we obtain the desired expression for the subsurface temperature anomaly T_s' in terms of the model thermocline depth anomaly $h(= \tilde{h} - \bar{h})$:

$$T_s' = T_s(h, \bar{h}) - T_s(h = 0, \bar{h}) \simeq \Gamma(\bar{h}) \cdot h, \tag{11}$$

where

$$\Gamma \equiv \left. \frac{\partial T_s}{\partial \tilde{h}} \right|_{\tilde{h}=\bar{h}} = \left. \frac{\partial cs}{\partial h_{20}^*} \right|_{f(\bar{h})} \cdot \left. \frac{\partial f}{\partial \tilde{h}} \right|_{\tilde{h}=\bar{h}}. \tag{12}$$

Figure 6 shows the annual average of Γ along the equator.⁵ Shown for comparison is the linearisation of the B88M parameterisation. As with the \bar{T}_z parameterisation the general shape of the old and new functions are broadly similar, but values for Γ using the new climatologies are larger especially in the east central Pacific (see Appendix for a discussion of the spike that is seen in the Γ derived using the FSU wind product).

Given that we are interested in the relationship between anomalies in the subsurface temperature due to anomalies in the thermocline displacement, it would seem that Γ could be obtained by simply regressing the observed anomalies in T_{50}^* against anomalies in \tilde{h} , with the latter calculated by forcing the 1.5 layer model with observed wind stress anomalies. Although the various analysis and observational datasets span a greater time than ever before, allowing for a much more accurate computation of the climatology, the ocean temperature data still lacks either

⁵ Since \bar{h} is the annual cycle, Γ has a unique annual cycle at each longitude, although for simplicity we use the annual mean value of Γ in LOAM.

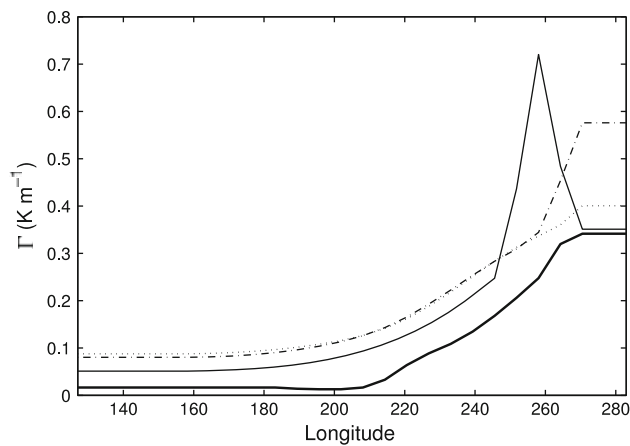


Fig. 6 The annual averaged $\Gamma(x)$ derived using: BOM subsurface temperature with FSU wind stress, *solid*, and with NCEP wind stress, *dash-dotted*. The *dotted* line is for the SODA subsurface data forced with NCEP wind anomalies. The *bold solid* line shows the linearisation of the B88 parameterisation

the quality or the time span for a reliable estimate of Γ directly from the anomalies in T_{50} and h_{20} . Thus, the climatological annual cycles of T_{50}^* and \tilde{h} were used to estimate Γ .

We have now devised functions that fit Γ and \bar{T}_z to the data. Before we can calculate K_w and K_T , we note that these functions contain the multipliers δ_w and δ_T , respectively. These represents processes that are unresolved in the crude 1.5 layer model. For example, the mixed layer depth is not constant across the equator (assumed in the ocean model), thus the amount of mixing into the top 50 m of the ocean is also not constant. In both the ZCM and B88M, δ_w and δ_T are set equal to 0.75. There is no a priori reason to expect that δ_T and δ_w are the same, however, as K_w and K_T represent very different processes that have rich spatial structures. For example, along the equator stratification and shear is much weaker in the western Pacific than in the eastern Pacific. Therefore, using the same single value for δ_w and δ_T at all points in the ocean is not likely to be optimal. In the next section we will describe how appropriate values for these constants may be determined.

3.2.3 Estimating δ_w and δ_T

In order to establish suitable values for δ_w and δ_T , we insert the new mean fields (currents and upwelling) and their respective parameterisations of Γ and \bar{T}_z into the linearised version of the ZCM ocean model that is used in LOAM. δ_w and δ_T in K_w and K_T are then set to various values between 0.1 and 1 in increments of 0.1, giving, in total, 100 different ocean models for each set of background states. In each model, δ_w and δ_T are the same for all points in latitude and longitude. Each of these 100 different ocean models is then forced by the time series of 1970–2005 NCEP wind

stress anomalies. The wind anomalies have been subjected to two passes of a 3-month running mean filter in order to remove the high frequency variability that is dominated by uncoupled physics. Each ocean model then computes the SST, and from this the nino3 index is calculated. Figure 7 summarizes the skill of the ocean models that use the SODA currents and temperature and NCEP wind stress. Each concentric ring on the diagram represents a line of constant RMSE; the angle down from the vertical represents the correlation. Note that the scaling for the correlation is not linear, rather the angle varies as the squared correlation. Points closest to the abscissa have the highest correlation between observations and simulations, and those closer to the origin have the lowest RMSE. Each of the coloured lines represents a set of models the same value for δ_w . Tick marks along those lines are at intervals of 0.1 δ_T , with δ_T varying between 0.1 and 1. Thus, the third tick from the end of the darkest blue line that is labelled 0.1, is an ocean model with $\delta_w = 0.1$ and $\delta_T = 0.3$. For clarity only lines of $\delta_w = 0.1, 0.2, 0.3$ are shown. The circle on Fig. 7 shows the skill of the model using $\delta_w = 0.6$ and $\delta_T = 0.1$. These are the values of δ_w and δ_T where the correlation between the modelled and observed nino3 is highest and the RMSE lowest, and, therefore the values for which the simulated nino3 index best fits the observed nino3 using spatially uniform (but different) values for δ_w and δ_T .

Upon examining similar diagrams averaging SST between 5°N and 5°S at each longitudinal point (not shown), it was observed that the values of δ_w and δ_T that

optimised SST locally were different at each longitudinal point. Therefore, the values of δ_w and δ_T that optimise the SST at each longitude point were then chosen to create $\delta_w(x)$ and $\delta_T(x)$, so now δ_w and δ_T vary with longitude. It is only necessary to calculate $\delta_w(x)$ and $\delta_T(x)$ along the equator: off the equator, the mean upwelling is extremely weak and so the values of δ_w and δ_T are inconsequential. As we go east to west along the equator, nino3 (and SST in general) is not especially sensitive to changing δ_w ; in contrast, quite different values of δ_T optimize the SST fit at each longitude point. Hence, the optimal values of δ_w and δ_T that optimize the local SST skill are nowhere equal to one another (by contrast, in ZCM the values of δ_w and δ_T were set to be equal and did not vary with latitude nor longitude).

The procedure for evaluating $\delta_w(x)$ and $\delta_T(x)$ that we use is somewhat subjective, but we should note that in the east Pacific, where the SST is most affected by local upwelling, the optimal values of $\delta_w(x)$ and $\delta_T(x)$ (i.e., those that maximise the correlation and minimise the RMSE) are easy to choose from the array of possible values. Furthermore, when the tuned ocean and atmosphere models are coupled, the behaviour of the coupled model is not especially sensitive to the choice of $\delta_w(x)$ and $\delta_T(x)$. The coupled model behaviour is more sensitive to the choice of Γ and $\overline{T_z}$ than to the choice of $\delta_w(x)$ and $\delta_T(x)$. Each of the ocean models uses a different set of Γ and $\overline{T_z}$ which yield very different K_w and K_T . Since the differences in K_w and K_T that arise from using different values of Γ and $\overline{T_z}$ are larger than the differences using the same Γ and $\overline{T_z}$ but different, and yet still plausible, values of δ_w and δ_T , choosing the values of δ_w and δ_T that give the best fit to the observed anomalies is not of paramount importance.

3.2.4 The final compilation

Now that all the terms in K_T and K_w can be calculated, we are in a position to be able to compile the ocean component of LOAM that best fits the observations. With the number of required background states and the number of different data sets available, a large number of possible model ocean model configurations can be constructed using various different combinations of backgrounds states and subsurface parameterisations. Rather than present and test all possible models, in the next section, when we couple the ocean and atmosphere, we will show just three ocean models. A summary of the data sets used in these three models is presented in Table 1. The values of K_w and K_T for these models are shown in Fig. 8. These three models represent the models that have K_T and K_w that lie at the extremes and middle of the distribution of possible K_T and K_w . These three ocean models will illustrate how sensitive the coupled model is to the values of these two coefficients (although there is no guarantee that these three ocean

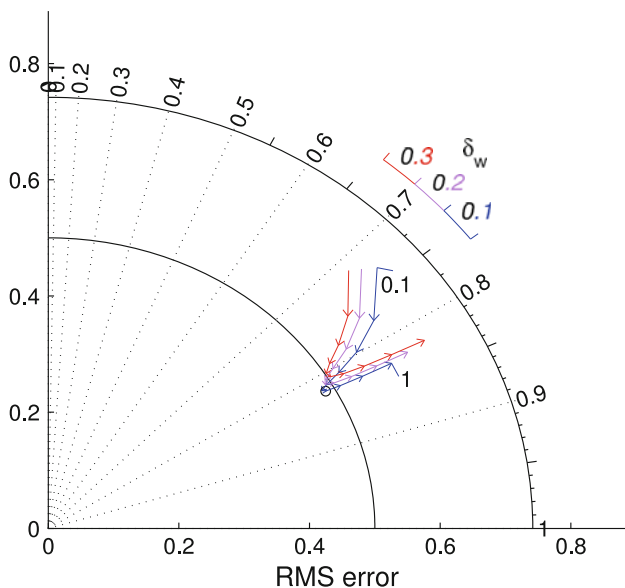
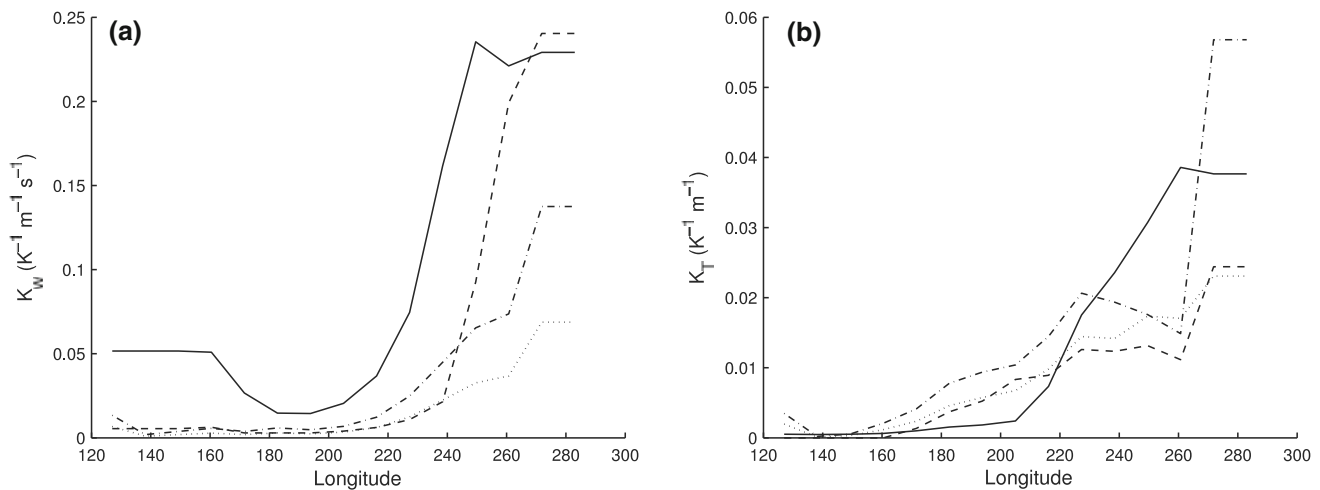


Fig. 7 Summary diagram for tuning the ocean model based on the SODA subsurface parameterisation forced with NCEP wind stress anomalies. The fit is between the observed and modelled nino3 index. See text for explanation of the diagram. The circle represents the model using δ_w and δ_T .

Table 1 Summary table of the background state fields used in the three example models

Model name	Data sets used			
	SST	Currents	Subsurface parameterisation	Wind stress
LOAM(T80)	RC	Derived from the 1.5 layer ocean forced with RC winds		RC
LOAM(a)	SODA	SODA	SODA	NCEP
LOAM(b)	NCEP	GODAS	BOM	FSU
LOAM(c)	NCEP	GODAS	BOM	NCEP

**Fig. 8** Longitudinal variations of **a** K_w and **b** K_T averaged between 5°N and 5°S. *Solid line* shows the functions using B88M background states and the *dashed line* LOAM(a), *dotted* LOAM(b) and *dash-dotted* LOAM(c) background states

models should also represent the largest spread in the behavior of the coupled models).

3.3 The atmosphere

With the ocean independently tuned to give the best fit to the data, the atmosphere still requires validation. To do this we shall compare the observed windspeed anomalies to those produced by the LOAM atmosphere component, forced by the observed SST anomalies.

The atmospheric component of LOAM is the linear atmosphere model due to Gill (1980) that includes a linearisation of the convergence feedback that was devised by Zebiak (1986). We force this model with the observed SST anomalies from 1970 to 2005 from the NCEP/OI dataset and calculate the resulting windspeed. This modelled windspeed and the NCEP zonal windspeed anomalies for the same period are then averaged over the central equatorial Pacific (10°N–10°S, 140°E–120°W). This spatial average was chosen because it matches the region that explains most of the variance on interannual timescales in both the Gill model and the NCEP data. The two timeseries are both smoothed by two passes of a 3-month running mean filter to remove the high frequency (non-SST related)

variability in the wind anomalies; the results are shown in Fig. 9. The correlation between the simulated and observed wind stress is 0.85, showing that over this region the Gill model with the linearised convergence feedback captures much of the variance in zonal wind anomalies over this region. However, the regression coefficient between these two series is 0.56, indicating that the model underestimates the zonal windspeed by a factor of 0.56. This is not surprising since the Gill model winds are an average over the whole lower tropopause, rather than the surface wind. Therefore, in order for the Gill model to give the correct surface wind stress to the force the ocean model we must rescale the wind stress.

Since the surface wind stress goes linearly with wind speed in the linearised model, the wind speed from the atmosphere model needs to be multiplied by approximately 1/0.56 in order to get the correct wind stress anomalies to force the ocean model. Assuming that the correct drag coefficient is 1.25×10^{-3} , in order to get the surface wind stress anomalies of the correct amplitude, the drag coefficient C_D used to couple the the atmosphere and ocean in the new versions of LOAM needs to be 2.1×10^{-3} (this is qualitatively similar to the value that was originally used in ZCM, 2.51×10^{-3}). We should note that the results in the

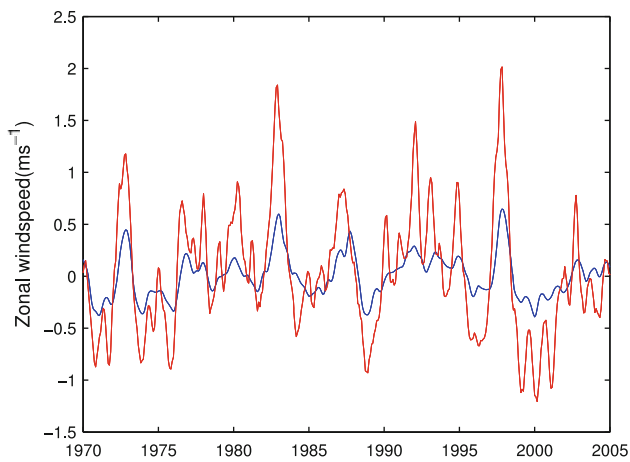


Fig. 9 The zonal wind speed anomalies averaged over 10°N–10°S, 140°E–120°W for NCEP/OI (*red line*) and for the Gill atmosphere with a linearised convergence feedback forced with NCEP SST anomalies (*blue line*)

next section are not particularly sensitive to the value of the drag coefficient.

3.4 Summary so far

We have shown in this section how to incorporate the observed climatological mean fields into LOAM. We have also shown how, in an uncoupled sense, we can tune the 1.5 layer ocean to give the best hindcast of SST anomalies when the model is forced by observed wind stress anomalies. Similarly, the drag coefficient in the atmosphere is

tuned to give the best fit of hindcast zonal wind stress anomalies over the equatorial waveguide when the atmosphere is forced by observed SST anomalies. Now all that remains is to couple the ocean and the atmosphere models and evaluate the coupled model behaviour.

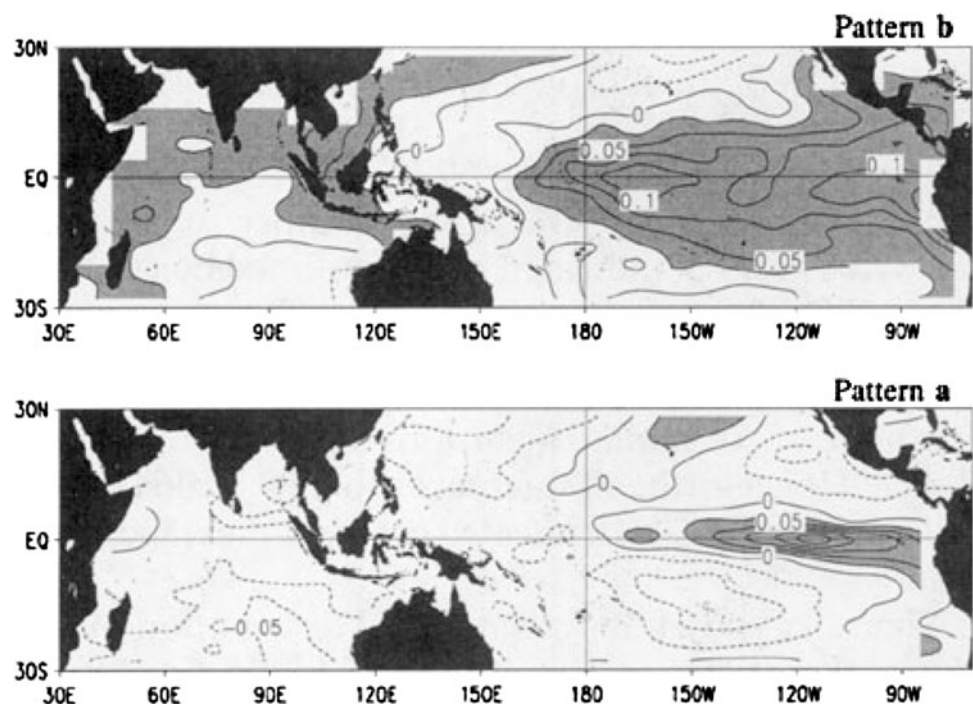
4 LOAM with new mean states

In this section we couple the atmosphere and ocean models that include the observed mean states (and tuned values of C_D , δ_w and δ_T) and examine the temporal and spatial structure of the leading (least decaying) mode of the coupled system. All constants and parameterisations that have not yet been discussed are set to the values used in the T80 version of LOAM; in particular, realistic values for the western boundary reflection and ocean mechanical damping (see Thompson and Battisti 2000). Table 1 summarizes the background states of the three candidate models that we shall discuss in this section.

4.1 Primary results

When we decompose LOAM with the new mean states into its Floquet modes, we find that the first mode resembles the canonical pattern associated with ENSO (compare Figs. 10, 11): hence, the ENSO mode exists using the more realistic mean states. The period of the ENSO mode using the new mean states ranges from 3.7 to 4.9 years, which compares favorably to that estimated from a linear inverse model fit to

Fig. 10 The ENSO mode reproduced from Penland and Sardeshmukh (1995). The mode evolves $b \rightarrow a \rightarrow -b \rightarrow -a \rightarrow b$ over 3.8 years. The contour interval is arbitrary but the same in each panel



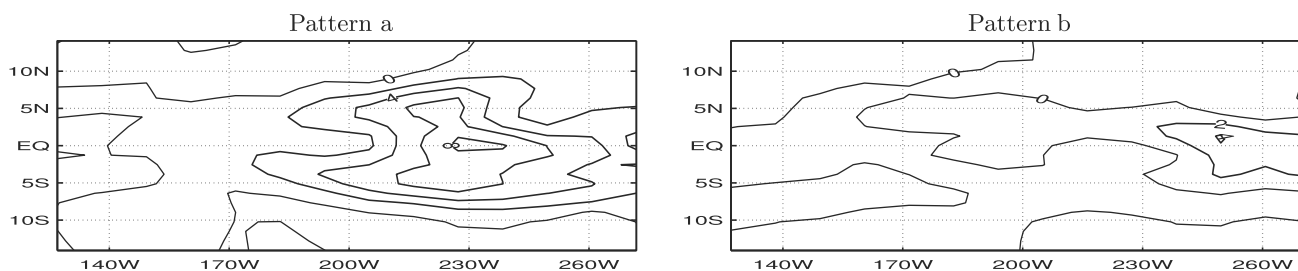


Fig. 11 The SST part of the ENSO mode from the LOAM with the SODA/NCEP climatological mean fields and tunings. The mode evolves $a \rightarrow b \rightarrow -a \rightarrow -b \rightarrow a$ over 3.7 years. The contour interval is arbitrary but the same in each panel

the observations (3.5–4.1 years; see Table 2). The damping rate using the new mean fields ranges from 0.34 to 0.53 year⁻¹, which also compares favorably to that estimated from observations (0.22–0.63 year⁻¹). In Table 2 we see that for all estimates of the mean state, the ENSO mode is stable and is also damped more than the ENSO mode that results from LOAM using the same T80 parameter set but with the mean state fields from the original ZCM (LOAM(T80)). We recall that the method for calculating the background states and for tuning the three parameters C_D , δ_w and δ_T made no assumptions about the behaviour of the components when they were coupled. Thus, we had no a priori reason to expect that the ENSO mode would exist. That it does exist and that it is stable lends weight to the hypothesis that the ENSO mode in nature is truly a coupled atmosphere–ocean mode and it is stable.

Table 2 The temporal properties of the ENSO mode for various observational data sets and model runs

Model	ENSO mode		Variance (%)		Noise (SD)
	Growth (year ⁻¹)	Period (years)	EOF 1	EOF 2	
Kaplan	0.63 (a)	4.1 (a)	50	9.2	
	0.53 (b)	3.5 (b)			
NCEP/OI	0.22 (c)	3.8 (c)	45	12	
B88M	1.82	2.8	92	4.2	–
LOAM(T80)	0.80	3.8	83	3.5	0.20
LOAM(a)	0.53	3.7	48	6.7	0.33
LOAM(b)	0.48	4.2	42	4.7	0.52
LOAM(c)	0.34	4.9	34	3.8	0.42

The modal period and annual growth from the models are from the first Floquet mode of the linearized model; those from observations are estimated using a linear inverse model with data from (a) COADS and (b) NCEP/OI by Johnson (1999) and from (c) COADS by Penland and Sardeshmukh (1995). Also indicated is the percent of total variance explained by the first two EOFs of SST in the tropical Pacific for each observation product and for each LOAM under stochastic forcing

The last column is the amplitude of the (SST) stochastic forcing that, when applied to each LOAM, renders variance in the simulated nino3 identical to that observed

In order to run LOAM as a time varying model, it must be forced. As with LOAM(T80), the three candidate models were all forced by applying white noise to the SST field. The amplitude of the noise applied to each model is adjusted such that the model produces a nino3 index that has the same variance as that observed; the amplitude of the noise (measured by one standard deviation) varies from 0.33 to 0.5°C for each model. Table 2 summarises how much of the SST variance is contained in the first two EOFs. It also summarises the annual growth rate and period of the ENSO mode under each mean state, taken from the annual propagator matrix. [Note that the ENSO mode has a rich frequency spectrum, though the dominant frequency is determined from the eigenvalue of the annual propagator matrix (e.g., Thompson and Battisti 2000)].

When each model is stochastically forced we find that the first EOF of SST resembles the first EOF of the observed SST (Fig. 12). The local maximum in the first EOF in all the new models is shifted toward the central east Pacific rather than in the far east, where B88M and LOAM(T80) place it. This westward displacement is mainly due to the shift in the spatial distribution of K_w and K_T from the old to new parameterisations. The amplitude of both K_w and K_T is smaller in the far east in the new formulations than in the old (Fig. 8). This makes the ocean less responsive to anomalies in vertical advection and thus shifts the peak in SST variance farther to the west, closer to that observed.

The fraction of total variance in SST associated with the first EOF from the models and observations is also indicated in Table 2. The variance explained by the first EOF of the three models ranges from 34 to 48% (the same statistic from the model with the old mean fields ranges from 83 to 92%). This compares favorably to the fraction of variance in the first EOF from the observations (45 and 50%). However, the pattern of the first EOF from the each of the models with the new mean states features an equatorial SST maximum that is too confined to the equator when compared to either the observation-based EOF or the leading EOF from the model with the original mean state fields. This difference between the leading EOF of SST

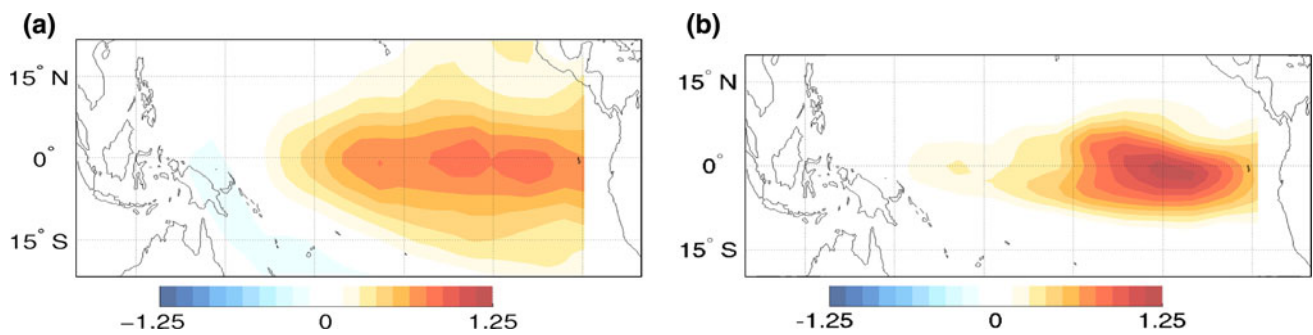


Fig. 12 EOF 1 of SST from **a** observations (Kaplan) and from **b** the stochastically forced LOAM(a). Contours are in $^{\circ}\text{C}$

from the new mean states and the old is not large and can be explained mostly by the stronger off equatorial currents in the original mean states (see Fig. 2). Along the equator, the second EOF from the LOAM with the new mean states is also qualitatively similar to the that from the observations (Fig. 13), featuring a distinctive east-to-west see-saw pattern that is absent in B88M and T80 (not shown). The models do not, and indeed cannot, capture the off equatorial parts of the observed second EOF because the SST anomalies in these regions are due to anomalies in the surface turbulent fluxes that are mainly due to anomalies in the surface wind speed (in LOAM, the surface heat flux anomaly is exactly proportional to the SST anomaly and independent of wind speed anomalies).

That the ENSO mode is stable lends weight to the hypothesis put forward by Penland and Sardeshmukh (1995) and supported by several studies: in nature, ENSO can be thought of as being a stable linear mode that is forced by noise (see also Chang et al. 1996; Johnson et al. 2000; Thompson and Battisti 2001; Philander and Fedorov 2003). In the original ZCM the ENSO mode was unstable. It is possible that the stability of the ENSO in all the versions of LOAM presented here may be explained not by the more accurate background states and subsurface parameterisations, but by the lower drag coefficient, western boundary reflection and higher mechanical damping [the T80 parameter set of Thompson and Battisti (2000)], all of which will tend damp the ENSO mode in ZCM. However,

this is not the case. When the original values of these parameters are used in LOAM along with the new background states, we find that in all cases the ENSO mode is stable (although in each case the mode is less stable than when using the more realistic values of western boundary reflection, ocean mechanical damping and the drag coefficient). This suggests that the ENSO mode is unstable in the original ZCM mainly because of the prescribed mean state fields that were used and that differ qualitatively from those observed (see Figs. 1, 2).

4.2 Further analysis of the impact of observed mean states on ENSO

We have incorporated more realistic climatological mean states in ocean currents, upwelling, SST and surface wind stress into the linearized coupled model, as well as changed three parameters in the coupled model by independent tuning of the uncoupled atmosphere (one parameter) and ocean (two parameters) modules. In Table 3 we show how changes in the atmosphere mean state and ocean mean state separately affect the growth rate and period of the leading (ENSO) mode. Here, we only show results using the SODA estimates of the ocean mean states along with the atmosphere mean state changes to create LOAM(a).

Starting from LOAM(T80) in which the original estimates of the atmosphere and ocean mean states were used, we first replace the mean state SST with that from the

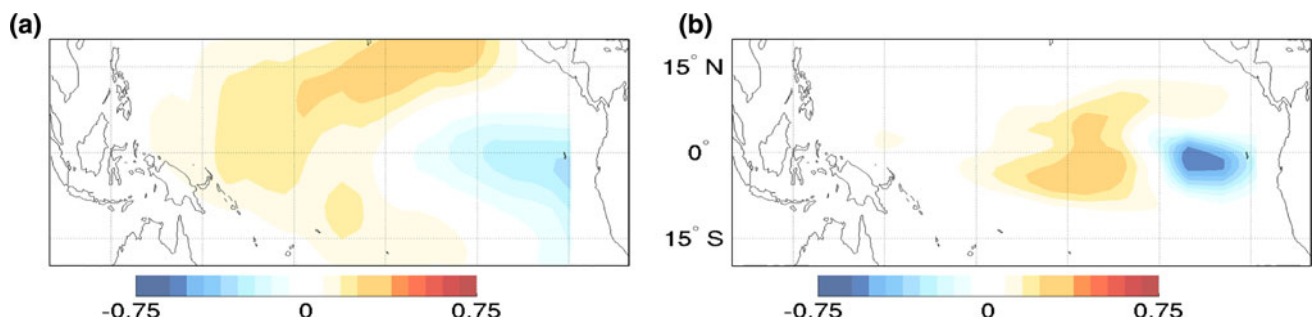


Fig. 13 EOF 2 of SST from **a** observations (Kaplan) and from **b** the stochastically forced LOAM(a). Contours are in $^{\circ}\text{C}$

Table 3 The impact of different mean state updates on the growth rate and period of the leading (ENSO) mode in LOAM

Experiment name	Description	Growth (year ⁻¹)	Period (year)
LOAM(T80)	Original mean fields	0.80	3.8
LOAM(a)	Observed mean fields	0.53	3.7
Exp a	T80 + SODA SST	0.89	3.5
Exp b	T80 + SODA Winds	0.86	3.8
Exp c1	T80 + SODA horizontal currents	0.49	4.5
Exp d	T80 + SODA upwelling, Γ and δ	0.32	3.3
Exp e	T80 + SODA SST and winds	1.09	3.3
Exp c2	T80 + SODA zonal currents	0.77	4.2
Exp c3	T80 + SODA meridional currents	0.57	4.0

The experiment LOAM(T80) refers to the results from the linearized ZCM using updates for western boundary reflection efficiency as in Thompson and Battisti (2000) and the estimates for all mean state fields that are used in the original ZCM

The LOAM(a) refers to the results from the same linearized model, but using the SODA observed mean state fields (including wind, SST and all currents) and updated estimates of the parameters

The remaining experiments use T80 mean fields except where noted. For example, *experiment e* uses currents and upwelling mean fields identical to those in the original ZCM and in LOAM, but SST and wind mean fields from SODA

SODA product—leaving all currents and winds to be the original estimates (experiment a in Table 3). This renders an ENSO mode that is slightly less stable (0.89 year⁻¹) and has a shorter period (3.5 year) than in LOAM(T80) (0.80 year⁻¹ and 3.8 year, respectively). A similarly subtle change to the ENSO mode is found when the original mean state winds used in T80 are replaced with the updated mean state climatological winds, experiment (b).

The effect of replacing the original mean state horizontal surface currents with those observed (SODA) (experiment c1) is much more profound: the period of the ENSO mode increases from 3.8 to 4.5 years and the mode is greatly stabilized, from 0.80 to 0.49 year⁻¹. The mean state currents in SODA are in general weaker than in the original ZCM which (all else being equal) renders thermocline displacements more important for creating SST anomalies and this increases the period of the ENSO mode (Fedorov and Philander 2001). It is interesting to note that the period and growth rate are sensitive to updates in the zonal currents, and particularly sensitive to updates in the meridional currents (cf., experiments c1, c2 and c3).

More realistic upwelling and values for the vertical mixing parameters (Γ and δ) also have a large impact on the ENSO mode properties. Replacing the upwelling field and the δ parameters with their SODA equivalents and leaving all horizontal currents, winds and SST to be the original mean states (experiment d) renders an ENSO mode that is much more stable (0.32 year⁻¹ vs. 0.80 year⁻¹) and has a shorter period (3.3 years vs. 3.8 years) than in LOAM(T80) because upwelling along the equator in the SODA product is weaker than that in the original estimate of upwelling used in LOAM(T80) and the ZC model.

The observed mean state in the ocean is clearly of paramount importance for rendering the ENSO mode to be

much more stable than in the original ZCM. Nonetheless, updates to the mean state SST and wind fields have a significant impact on ENSO, as indicated by contrasting the growth rate and period of ENSO when the original mean state SST and wind climatology are placed in LOAM (experiment e), which actually causes the ENSO mode to be unstable (1.09 years) and have a greatly shortened period compared to the model with the original means states (3.3 years vs. 3.8 years). Experiment e also serves to illustrate the richness in the response of ENSO to changes in the mean state: changing SST and winds independently has only a modest affect on the growth rate and period of ENSO (cf. LOAM(T80) with experiments a and b), while changing SST and winds simultaneously increases the growth rate and reduces the period of the ENSO mode by 25% or so.

5 Conclusions and discussion

Intermediate models of the coupled tropical atmosphere–ocean system have been used for over 20 years. They were first used to illuminate the physics of interannual climate phenomenon such as ENSO in the tropical Pacific and its Atlantic cousin, but these models continue to be used and be useful for a variety of reasons, including explorations how the tropical basin might respond to an external forcing such as changing insolation (Milankovitch) or atmospheric carbon dioxide. Importantly, most of the intermediate models are constructed as anomaly models, where anomalies are taken about a climatological mean state which is typically prescribed on a rather ad hoc basis. For example, the mean state SST and wind are often prescribed to be that observed, but the climatological ocean currents (including

upwelling) are approximated by forcing a reduced gravity model with the observed annual cycle of wind stress. A consistent lesson from studies using intermediate models, however, is that the temporal and spatial structure of the coupled modes and interannual variability in the tropics is extremely sensitive to the structure in the climatological mean states.

In this study we show how the observed climatological mean state fields (ocean currents and upwelling, atmospheric surface winds) can be incorporated into a linearized intermediate model of the tropical coupled atmosphere–ocean system: the linearized Zebiak and Cane model. Though the mean fields are entirely from observations, there remains three free parameters: two in the ocean and one in the atmosphere. We chose these parameters by forcing the ocean model with the observed wind stress anomalies and fit the simulated SST anomalies to those observed, and by forcing the atmosphere model with the observed SST anomalies and fit the simulated zonal wind stress anomalies along the equator in the central Pacific to those observed. The fitting of the ocean model and the atmosphere model are done prior to coupling.

We then coupled the ocean and atmosphere model and calculated the leading Floquet mode of the coupled atmosphere–ocean system and compared it to that found in the ZCM model using the original mean state fields. We found that the essential physics of the leading Floquet mode is very similar to the observed ENSO (mode) and is very similar to the ENSO mode in the original ZCM (see, e.g., Thompson and Battisti 2000). The period of the ENSO mode supported by the observed mean states is about 3.7–4.9 years, similar to that observed (3.5–4.1 years). Along the equator, the spatial structure of the ENSO mode is similar to the observed ENSO mode (and closer to the observed ENSO mode than when the original ZCM mean states are used). Unlike the original ZCM mean states, however, the observed mean fields clearly support an ENSO mode that is stable to perturbations. Thus, our results provide further evidence that ENSO is generated and maintained by stochastic (uncoupled) perturbations, as first proposed by Penland and Sardeshmukh (1995).

We reported on a series of experiments in which selected mean state variables were updated in the linearized atmosphere–ocean model while holding the remaining mean state fields fixed to be the original estimates. These experiments demonstrated that replacing the mean state ocean fields used in the original ZCM with the observed mean state fields had the greatest impact on the growth rate and period (and structure) of the ENSO mode. Updates in both horizontal and vertical currents had a large impact on the spatial and temporal structure of the ENSO mode; updates to the climatological SST and surface wind fields had somewhat of a lesser impact on the ENSO mode. This

was expected: at the time the ZCM model was constructed, there were reasonable data available to determine the SST and surface wind climatology, but there were insufficient data to calculate an accurate climatology of ocean currents and upwelling. Hence, the authors of the ZCM had to settle for sensible, albeit crude, estimates of these fields.

Since the first successful simulation of a realistic ENSO in a coupled atmosphere–ocean model by Zebiak and Cane (1987), scores of investigators have created simple, low dimensional toy models of the coupled atmosphere–ocean system in the tropical Pacific that grossly feature aspects of the mean state that are widely thought to be important for ENSO. Notable examples include Schopf and Suarez (1988); Battisti and Hirst (1989); Jin (1997) and Burgers et al. (2005). Similarly, investigators have searched for a small suite of mean state parameters that would be good indicators of how ENSO would change due to some externally forced change in the mean state: examples include Fedorov and Philander (2001); Collins (2005) and Guilyardi (2006). It is tempting to invoke the concepts and indices derived from these studies to explain *post facto* why ENSO changed in a series of GCM experiments in which the mean states were forced to change (for example, why ENSO changes in a climate model whereby the modern day insolation is replaced by that observed in the early Holocene, or the modern day greenhouse gas concentration is replaced by that anticipated at the end of this century). The sensitivity experiments presented in Sect. 4.2 make it clear, however, that changes in the spatial and temporal characteristics of ENSO can result from subtle changes in all of the mean state variables (as well as changes in the structure and amplitude of the external stochastic forcing). Hence, the only way to quantify and isolate the impact of changes in any particular field is to use a model that includes the temporal and spatial detail associated with the annual cycle in all of the important mean state fields: SST, surface winds, three dimensional currents and upper ocean thermal structure.

The method that we outline may be used to assimilate any set of ocean and atmosphere data into the LOAM. In a companion paper (Roberts et al. 2010), we incorporate the climatological mean states simulated by global climate models into LOAM and then use the latter to diagnose the physics of the leading coupled mode supported by the full climate models. Specifically, we use the climatological mean fields simulated by the CCSM and the HadCM3 under three different forcing scenarios: modern day, early Holocene and Last Glacial Maximum boundary conditions. We show that the linear model reproduces the changes in ENSO simulated by the full climate models and use the linear model to illuminate how and why the structure and variance in the ENSO mode changed in the full model. Interestingly, though the two climate models simulate

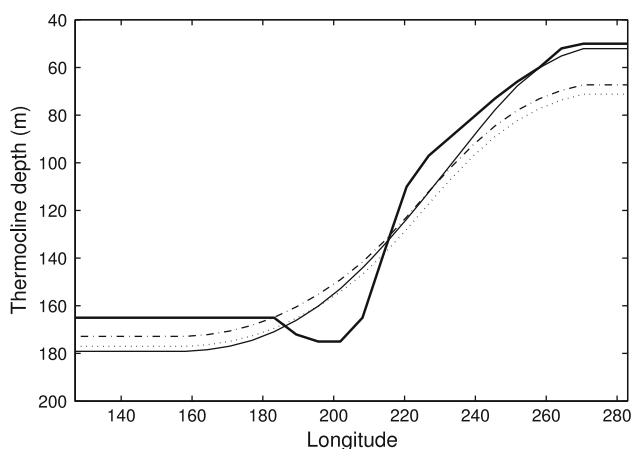


Fig. 14 Mean thermocline depth, \bar{h}_{20} , using $f(\bar{h})$ derived from \bar{h} and: the BOM subsurface temperature with FSU wind stress, solid line; the BOM subsurface temperature with NCEP wind stress, dash-dotted line; and the SODA subsurface data forced with NCEP wind anomalies, dotted line. Bold solid shows the ZC original

similar changes in ENSO variance (both show reduced variance during the early Holocene and enhanced variance during the LGM), analyses using the linearized model shows that they do so for very different reasons.

Acknowledgments This work was funded by a grant from the Ocean and Atmosphere Research (OAR) Climate Program Office (CPO) of the National Oceanic and Atmospheric Administration (NA08OAR4310883). We thank an anonymous reviewer for critical and constructive comments, and Sandy Tudhope and Daniel Vimont for thoughtful comments throughout our investigation.

Appendix: Comments on the empirically derived function Γ

In Fig. 6 there is a spike in the function Γ (which maps T_s to \bar{h} ; see Eq. 12) derived from the BOM temperature and FSU wind stress data at 260°E. This is explained by the shape of the function $cs(h_{20}^*)$. In Eq. 12 we see that Γ is a function of the gradient of $cs(h_{20}^*)$. As can be seen in Fig. 5, at thermocline depths of around 50 m, the gradient of $cs(h_{20}^*)$ is at its steepest: deeper and shallower than 50 m, the gradient of $cs(h_{20}^*)$ becomes less. When the FSU data is used to derive the values of $h_{20}^* = f(\bar{h})$ at which we evaluate $\frac{\partial cs}{\partial h_{20}^*}$, this function is evaluated very close to this inflection point—so close in fact that in the far east of the basin we cross the inflection point. Therefore, the gradient of $cs(h_{20}^*)$ increases and then decreases as we traverse the basin. This behaviour is peculiar to $f(\bar{h})$ derived from the FSU windstress product because it alone produces very shallow thermocline depths in the far eastern Pacific. This can be seen in Fig. 14 which shows $h_{20}^* = f(\bar{h})$, derived using values of \bar{h} calculated by forcing the 1.5 layer ocean with the observed seasonal cycle of wind stress from a

number of combinations of temperature and wind stress data. Figure 14 demonstrates the general result that using the FSU wind stress results in a h_{20}^* in the eastern Pacific that is 20 m shallower than that using due the NCEP dataset. This is due to the stronger equatorial easterlies in the FSU dataset (Wittenberg 2004).

References

- Battisti DS (1988) Dynamics and thermodynamics of a warming event in a coupled tropical atmosphere ocean model. *J Atmos Sci* 45(20):2889–2919
- Battisti DS, Hirst AC (1989) Interannual variability in a tropical atmosphere ocean model—influence of the basic state, ocean geometry and nonlinearity. *J Atmos Sci* 46(12):1687–1712
- Behringer D, Xue Y (2004) Evaluation of the global ocean data assimilation system at NCEP: The Pacific Ocean. In: Eighth symposium on integrated observing and assimilation systems for atmosphere, oceans, and land surface, AMS 84th Annual Meeting, Washington State Convention and Trade Center, Seattle, Washington
- Bourassa M, Smith S, O'Brien J (2001) A new FSU winds and flux climatology. In: 11th Conference on interactions of the sea and atmosphere, San Diego, CA, Am Meteorol Soc
- Burgers G, Jin FF, van Oldenborgh GJ (2005) The simplest ENSO recharge oscillator. *GRL*, Austin
- Carton JA, Chepurin G, Cao X (2000a) A simple ocean data assimilation analysis of the global upper ocean 1950–1995, part 2: results. *J Phys Oceanogr* 30:311–326
- Carton JA, Chepurin G, Cao X, Giese B (2000b) A simple ocean data assimilation analysis of the global upper ocean 1950–1995, part 1: methodology. *J Phys Oceanogr* 30:294–309
- Chang P, Ji L, Li H, FLugel M (1996) Chaotic dynamics versus stochastic processes in El Niño–Southern Oscillation in coupled ocean–atmosphere models. *Physica D* 98(6–7):301–320
- Collins M (2005) El Nino- or La Nina-like climate change? *Clim Dyn* 24(1):89–104
- Fedorov A, Philander SG (2001) A stability analysis of tropical ocean–atmosphere interactions: bridging measurements and theory for El Niño. *J Clim* 14:3086–3101
- Gill AE (1980) Some simple solutions for heat-induced tropical circulation. *Quart J Roy Meteorol Soc* 106(449):447–462
- Guilyardi E (2006) El Niño–mean state–seasonal cycle interactions in a multi-model ensemble. *Clim Dyn* 26:329–348
- Guilyardi E, Wittenberg A, Fedorov A, Collins M, Wang C, Capotondi A, van Oldenborgh GJ, Stockdale T (2009) Understanding El Niño in ocean–atmosphere general circulation models: progress and challenges. *Bull Am Meteorol Soc* 90:325–340
- Jin FF (1997) An equatorial recharge paradigm for ENSO. I. Conceptual model. *J Atmos Sci* 54:811–29
- Johnson SD (1999) Markov model studies of the El Niño–Southern Oscillation. PhD thesis. University of Washington
- Johnson SD, Battisti DS, Sarachik ES (2000) Empirically derived Markov models and prediction of tropical Pacific sea surface temperature anomalies. *J Clim* 13(1):3–17
- Johnson G, McPhaden M, Firing E (2001) Equatorial Pacific ocean horizontal velocity, divergence and upwelling. *J Phys Oceanogr* 31:839–849
- Kalnay E, Kanamitsu M, Kistler R, Collins W, Deaven D, Gandin L, Iredell M, Saha S, White G, Woollen J, Zhu Y, Chelliah M,

- Ebisuzaki W, Higgins W, Janowiak J, Mo K, Ropelewski C, Wang J, Leetmaa A, Reynolds R, Jenne R, Joseph D (1996) The NCEP/NCAR 40-year reanalysis project. *Bull Am Meteorol Soc* 77(3):437–470
- Mantua NJ, Battisti DS (1995) Aperiodic variability in the Zebiak-Cane coupled ocean–atmosphere model: air–sea interactions in the western equatorial Pacific. *J Clim* 8(12):2897–2927
- McPhaden M, Busalacchi AJ, Cheney R, Donguy JR, Gage KS, Halpern D, Ji M, Julian P, Meyers G, Mitchum GT, Niiler PP, Picaut J, Reynolds RW, Smith N, Takeuchi K (1998) The Tropical Ocean Global Atmosphere (TOGA) observing system: a decade of progress. *J Geophys Res* 103:14,169–14,240
- Neelin JD, Battisti DS, Hirst AC, Jin FF, Wakata Y, Yamagata T, Zebiak SE (1998) ENSO theory. *J Geophys Res* 103(14):261–290
- Penland C, Sardeshmukh PD (1995) The optimal-growth of tropical sea–surface temperature anomalies. *J Clim* 8(8):1999–2024
- Philander SG, Fedorov A (2003) Is El Niño sporadic or cyclic? *Ann Rev Earth Planet Sci* 31:579–594
- Philander SGH, Pacanowski RC, Lau NC, Nath MJ (1992) Simulation of ENSO with a global atmospheric GCM coupled to a high-resolution, tropical Pacific Ocean GCM. *J Clim* 5(4):308–329
- Poulain PM (1993) Estimates of horizontal divergence and vertical velocity in the equatorial Pacific. *J Phys Ocean* 23:601–607
- Rasmusson EM, Carpenter TH (1982) Variations in tropical sea surface temperature and surface wind fields associated with the Southern Oscillation/El Niño. *Mon Wea Rev* 110:354–384
- Reynolds RW, Rayner NA, Smith TM, Stokes DC, Wang W (2002) An improved in situ and satellite SST analysis for climate. *J Clim* 15:1609–1625
- Roberts WHG, Battisti DS, Tudhope AW (2010) Processes responsible for reduced ENSO variance in the LGM and early Holocene in CCSM3 and HadCM3. *J Clim* (to be submitted)
- Schopf PS, Suarez MJ (1988) Vacillations in a coupled ocean–atmosphere model. *J Atmos Sci* 45:549–566
- Seager R, Zebiak SE, Cane MA (1988) A model of The tropical Pacific sea–surface temperature climatology. *J Geophys Res* 93(C2):1265–1280
- Smith NR (1995a) An improved system for tropical ocean sub-surface temperature analyses. *J Atmos Ocean Technol* 12:850–870
- Smith NR (1995b) The BMRC ocean thermal analysis system. *Aust Meteorol Mag* 44:93–110
- Thompson CJ (1998) A linear, stochastic, dynamical model of El Niño–Southern Oscillation. PhD thesis. University of Washington
- Thompson CJ, Battisti DS (2000) A linear stochastic dynamical model of ENSO. Part I. Model development. *J Clim* 13(15):2818–2832
- Thompson CJ, Battisti DS (2001) A linear stochastic dynamical model of ENSO. Part II. Analysis. *J Clim* 14(4):445–466
- van Oldenborgh G, Philip SY, Collins M (2005) El Niño in a changing climate: a multi-model study. *Ocean Sci* 1:81–95
- Wittenberg AT (2004) Extended wind stress analyses for ENSO. *J Clim* 17(13):2526–2540
- Zebiak SE (1986) Atmospheric convergence feedback in a simple model for El Niño. *Mon Wea Rev* 115(7):1263–1271
- Zebiak SE, Cane MA (1987) A model El-Niño Southern Oscillation. *Mon Wea Rev* 115:2262–2278